REPORT DOCUMENTATION PAGE

Form Approved OMB NO. 0704-0188

1. REPORT DATE (DD-MM-YYYY)	2. REPORT TYPE	3. DATES COVERED (From - To)
18-09-2008	Final Report	11-Sep-2006 - 10-Jun-2008

4. TITLE AND SUBTITLE
Prestall Behavior of a Transonic Axial Compressor Stage via Time-Accurate Numerical Simulation

5a. CONTRACT NUMBER
W911NF-06-1-0447

5b. GRANT NUMBER

5c. PROGRAM ELEMENT NUMBER
611102

6. AUTHORS
Jen-Ping Chen, Michael D. Hathaway, Gregory P. Herrick

5d. PROJECT NUMBER

5e. TASK NUMBER

5f. WORK UNIT NUMBER

7. PERFORMING ORGANIZATION NAMES AND ADDRESSES
Ohio State University Research Foundation
Office of Sponsored Programs
Ohio State University Research Foundation
Columbus, OH 43210 -1063

8. PERFORMING ORGANIZATION REPORT NUMBER

9. SPONSORING/MONITORING AGENCY NAME(S) AND ADDRESS(ES)
U.S. Army Research Office
P.O. Box 12211
Research Triangle Park, NC 27709-2211

10. SPONSOR/MONITOR'S ACRONYM(S)
ARO

11. SPONSOR/MONITOR'S REPORT NUMBER(S)
49625-EG.1

12. DISTRIBUTION AVAILIBILITY STATEMENT
Approved for Public Release; Distribution Unlimited

13. SUPPLEMENTARY NOTES
The views, opinions and/or findings contained in this report are those of the author(s) and should not contrued as an official Department of the Army position, policy or decision, unless so designated by other documentation.

14. ABSTRACT
CFD calculations using high-performance parallel computing were conducted to simulate the pre-stall flow of a transonic compressor stage, NASA compressor Stage 35. The simulations were run with a full-annulus grid that models the 3D, viscous, unsteady blade row interaction without the need for an artificial inlet distortion to induce stall. The simulation demonstrates the development of the rotating stall from the growth of instabilities. Pressure-rise performance and pressure traces are compared with published experimental data before the study of flow evolution prior to the rotating stall. Spatial FFT analysis of the flow indicates a rotating long-length disturbance of one rotor circumference, which is followed by a spike-type

15. SUBJECT TERMS
CFD, turbomachinery, compressor, rotating stall

16. SECURITY CLASSIFICATION OF:			17. LIMITATION OF ABSTRACT	15. NUMBER OF PAGES	19a. NAME OF RESPONSIBLE PERSON
a. REPORT	b. ABSTRACT	c. THIS PAGE			Jenping Chen
U	U	U	SAR		19b. TELEPHONE NUMBER 614-247-8854

Report Title

Prestall Behavior of a Transonic Axial Compressor Stage via Time-Accurate Numerical Simulation

ABSTRACT

CFD calculations using high-performance parallel computing were conducted to simulate the pre-stall flow of a transonic compressor stage, NASA compressor Stage 35. The simulations were run with a full-annulus grid that models the 3D, viscous, unsteady blade row interaction without the need for an artificial inlet distortion to induce stall. The simulation demonstrates the development of the rotating stall from the growth of instabilities. Pressure-rise performance and pressure traces are compared with published experimental data before the study of flow evolution prior to the rotating stall. Spatial FFT analysis of the flow indicates a rotating long-length disturbance of one rotor circumference, which is followed by a spike-type breakdown. The analysis also links the long-length wave disturbance with the initiation of the spike inception. The spike instabilities occur when the trajectory of the tip clearance flow becomes perpendicular to the axial direction. When approaching stall, the passage shock changes from a single oblique shock to a dual-shock, which distorts the perpendicular trajectory of the tip clearance vortex but shows no evidence of flow separation that may contribute to stall.

List of papers submitted or published that acknowledge ARO support during this reporting period. List the papers, including journal references, in the following categories:

(a) Papers published in peer-reviewed journals (N/A for none)

Chen, J.P., Hathaway, M.D., Herrick, G.P., 'Pre-Stall Behavior of a Transonic Axial compressor Stage via time-Accurate Numerical Simulation,' in print, ASME Journal of Turbomachinery, Vol. 130, 041014, October,2008.

Number of Papers published in peer-reviewed journals: 1.00

(b) Papers published in non-peer-reviewed journals or in conference proceedings (N/A for none)

Number of Papers published in non peer-reviewed journals: 0.00

(c) Presentations

Number of Presentations: 0.00

Non Peer-Reviewed Conference Proceeding publications (other than abstracts):

Number of Non Peer-Reviewed Conference Proceeding publications (other than abstracts): 0

Peer-Reviewed Conference Proceeding publications (other than abstracts):

1. Cameron, J.D., Morris, S.C., Barrows, S.T., and Chen, J.P., “On the Interpolation of Casing Measurements in Axial Compressors,” ASME paper GT2008-51371.
2. Bennington, M.A., Cameron, J.D., Morris, S.C., Legault, C., Barrows, S.T., and Chen, J.P., McNulty, G.S., and Wadia, A.R., “Investigation of Tip-Flow Based Stall Criteria Using Rotor Casing Visualization,” ASME paper GT2008-51319.
3. Chen, J.P., Webster, R.S., Hathaway, M.D., Herrick, G.P., and Skoch, G.J., 2006, “Numerical Simulation of Stall and Stall Control in Axial and Radial Compressors,” AIAA paper 2006-418. AIAA Best Paper Award, AIAA Joint Propulsion Conference, Sacramento, CA, July 9-13, 2006.
4. Dear, C. and Chen, J.P.,’A Computational Validation Study of Parallel TURBO for Rotor 35,’ AIAA-2006-0420.

Number of Peer-Reviewed Conference Proceeding publications (other than abstracts): 4

(d) Manuscripts

Number of Manuscripts: 0.00

Number of Inventions:

Graduate Students

NAME	PERCENT_SUPPORTED
Sean Barrows	0.50
Benjamin Johnson	0.50
FTE Equivalent:	**1.00**
Total Number:	**2**

Names of Post Doctorates

NAME	PERCENT_SUPPORTED
FTE Equivalent:	
Total Number:	

Names of Faculty Supported

NAME	PERCENT_SUPPORTED	National Academy Member
Jen-Ping Chen	0.20	No
FTE Equivalent:	**0.20**	
Total Number:	**1**	

Names of Under Graduate students supported

NAME	PERCENT_SUPPORTED
FTE Equivalent:	
Total Number:	

Student Metrics

This section only applies to graduating undergraduates supported by this agreement in this reporting period

The number of undergraduates funded by this agreement who graduated during this period: .....

The number of undergraduates funded by this agreement who graduated during this period with a degree in science, mathematics, engineering, or technology fields:.....

The number of undergraduates funded by your agreement who graduated during this period and will continue to pursue a graduate or Ph.D. degree in science, mathematics, engineering, or technology fields:.....

Number of graduating undergraduates who achieved a 3.5 GPA to 4.0 (4.0 max scale): .....

Number of graduating undergraduates funded by a DoD funded Center of Excellence grant for Education, Research and Engineering: .....

The number of undergraduates funded by your agreement who graduated during this period and intend to work for the Department of Defense .....

The number of undergraduates funded by your agreement who graduated during this period and will receive scholarships or fellowships for further studies in science, mathematics, engineering or technology fields: .....

Names of Personnel receiving masters degrees

NAME

Total Number:

Names of personnel receiving PHDs

NAME

Total Number:

Names of other research staff

NAME PERCENT_SUPPORTED

FTE Equivalent:

Total Number:

Sub Contractors (DD882)

Inventions (DD882)

Prestall Behavior of a Transonic Axial Compressor Stage via Time-Accurate Numerical Simulation

Jen-Ping Chen
The Ohio State University,
Columbus, OH 43210

Michael D. Hathaway

Gregory P. Herrick

Army Research Laboratory,
Vehicle Technology Directorate,
Cleveland, OH 44135

Computational fluid dynamics calculations using high-performance parallel computing were conducted to simulate the prestall flow of a transonic compressor stage, NASA compressor Stage 35. The simulations were run with a full-annulus grid that models the 3D, viscous, unsteady blade row interaction without the need for an artificial inlet distortion to induce stall. The simulation demonstrates the development of the rotating stall from the growth of instabilities. Pressure rise performance and pressure traces are compared with published experimental data before the study of flow evolution prior to the rotating stall. Spatial fast Fourier transform analysis of the flow indicates a rotating long-length disturbance of one rotor circumference, which is followed by a spike-type breakdown. The analysis also links the long-length wave disturbance with the initiation of the spike inception. The spike instabilities occur when the trajectory of the tip clearance flow becomes perpendicular to the axial direction. When approaching stall, the passage shock changes from a single oblique shock to a dual shock, which distorts the perpendicular trajectory of the tip clearance vortex but shows no evidence of flow separation that may contribute to stall. [DOI: 10.1115/1.2812968]

Introduction

Advances in gas turbine engine technology have made possible the production of highly efficient engines. However, the useful operating range of a gas turbine engine is limited by the stable operation of the compressor. The limiting instability can be characterized by either rotating stall or surge. Surge is the zeroth order planar oscillation mode resulting from overall imbalance of the entire propulsion system, thus, analysis would have to include full volume and ducting. This violent system instability may be preceded by a rotating stall, which sets up alternating stress on the blades. Rotating stall and surge can cause destructive damage to engines and should be avoided. Understanding the physical process of the onset of rotating stall can aid in the design of a better control method to stabilize the system and enhance engine performance.

Stall inception has been an active research effort for the past five decades. The events leading to rotating stall have been traditionally classified according to two different types of wave disturbances moving around the annulus: long-length (modal) and short-length (spike) waves. Long-length wave disturbances are those with length on the order of the rotor circumference. This type of disturbance is caused by the characteristic frequencies of the compression system. Theories to model the long-length instability were developed by Moore and Greitzer [1]. The assumption is that the disturbance length scale is much larger than one blade pitch, and that the entire blade row can be modeled, both spatially and temporally, without the knowledge of the detailed flow inside the blade passages. This approach predicts the existence of long-length waves leading to stall. McDougall [2] demonstrated the existence of the modal waves through experiments, and Garnier et al. [3] supported the validity of the Moore and Greitzer model with detailed measurements. Unsteady pressure or axial velocity measurements from probes placed around the annulus are usually used to track the development of modal waves. Modal oscillations often have an axial extent from inlet to exit. It is typically a 2D (θ,x) phenomenon, which is not an early form of stall cell but instead represents harmonic oscillations of the flow field. It usually appears when the shape of the total-to-static pressure rise characteristic becomes horizontal.

The second type of stall inception mechanism is the short-length, or spike, disturbances. These are disturbances with length scale on the order of blade passage breadth. Spikes can be viewed as embryonic stall cells with flow breakdown in local regions (Camp and Day [4]); it is a 3D phenomenon whose development depends on the flow structure within the blade passage. A common scenario for the spike stall inception process is that localized, 3D pockets of instability in multiple blade passages erupt first to form small-sized multicell rotating stall. These stall cells rotates at 30–85% rotor speed initially and then merge into a single rotating stall cell within a few rotor revolutions (Day [5]). The final speed of the consolidated stall cell is nearly half or less of the rotor speed (Cumpsty [6]). A spike disturbance more frequently occurs when the slope of the pressure rise characteristic is still negative. That is, the pressure still rises as the mass flow reduces.

The above discussions indicate that the slope of the pressure rise characteristic may correlate with the stall inception type. Spike and mode can also be the different aspects of the stall inception process and can exist in the same machine (Day [5]). Day indicated that modal waves may be measurable in the machine for as many as 200 rotor revolutions before stall. A spike disturbance, on the other hand, once formed, can lead to rotating stall quickly, usually within a few rotor revolutions.

Numerical simulation using computational fluid dynamics (CFD) techniques has been shown as an alternative way to analyze aerodynamic problems and is a complement to experiments in the understanding of complex flow phenomena. Flow structure can be examined in detail where experimental measurements are difficult or impossible. During the past ten years, steady-flow simulations have provided an increasingly accurate prediction of the flow up to the point of compressor stall. Attempts to study stall

Contributed by the International Gas Turbine Institute of ASME for publication in the JOURNAL OF TURBOMACHINERY. Manuscript received June 7, 2007; final manuscript received August 20, 2007; published online August 1, 2008. Review conducted by David Wisler. Paper presented at the ASME Turbo Expo 2007: Land, Sea and Air (GT2007), Montreal, Quebec, Canada, May 14–17, 2007.

through unsteady simulations of a periodic subset of the blades in a compressor blade row (Hoying et al. [7], Vo et al. [8], Davis and Yao [9]) or through reduced-order unsteady-flow models (Gong et al. [10]) have reached valuable findings of the flow structure leading to stall. However, since the temporal flow field variations that occur during stall inception are not harmonics of blade passing frequency, a full-annulus model should be used to remove the constraint of the periodic model in order to study the transition from a steady flow into the unsteady stalling flow, and to resolve flow features of length scale on the order of the rotor circumference. Such simulations have been done two dimensionally (He [11], Saxer-Felici et al. [12]), but stall and the instabilities leading to stall are inherently three-dimensional phenomena. Predicting stall phenomena may thus require three-dimensional unsteady full-annulus simulations, which is a daunting computational endeavor requiring considerable computational resources. Due to the rapid advance of high-performance computing in the past decade, advanced CFD codes have benefited from the almost-unlimited computing potential of parallel computing. Recently, Chen et al. [13] demonstrated the ability to conduct a full-annulus 3D unsteady computation of an entire compressor stage while Hah et al. [14] also conducted a full-annulus 3D computation of an isolated rotor. This trend indicates that large-scale simulation using parallel computing is within reach.

Previous comparisons of the time averages of unsteady phase-lag and partial annulus predictions to measurements have shown the validity of the TURBO code to capture the 1D and 2D characteristics of this compressor (Hathaway et al. [15]). The intent of this work is to use the available experimental data to provide assessment of the code and to show evidence that the computational model reasonably captures the inherent behavior of compressors as they are throttled into stall. It is recognized that some features of the actual tested compressor are not captured by the computational model, for example, the leakage gap at the rotor/stator hub interface, the actual blade tip profile, and the geometry of the upstream and downstream ducting between the plenum and throttle valve locations. Although these features might influence the actual compressor stall, they are not considered requisite to understanding fundamental stall inception characteristics.

Axial Compressor, Stage 35

NASA research single-stage compressor Stage 35, representative of the advanced transonic core compressor, is used in this investigation. A schematic of the compressor test rig and compressor geometry is provided in Fig. 1 and the design parameters are provided in Table 1. Stage 35 produces 1.8 total pressure ratio at a mass flow rate of 20.2 kg/s at the design speed of 17,189 rpm. Details of the Stage 35 geometry, operating conditions, and the experimental results are provided by Reid and Moore [16].

Relevant Experimental Work

Time-resolved pressure measurement of Stage 35 near stall was reported by Bright et al. [17]. The experiment was performed at 85% design speed. Several configurations, including a clean-inlet case, were reported in that paper. For the interest of this study we will focus on the clean-inlet case. The compressor was transitioned into stall using a continuous throttle maneuver. Time-resolved pressure was recorded by high-frequency-response transducers at eight locations equally spaced around the annulus. Figure 2 reproduces the pressure traces of the clean-inlet case for 180 revolutions prior to stall reported in that paper (the original data are not available to us). Based on the pressure disturbance, Bright et al. [17] commented that the compressor with the clean-inlet stalls due to modal instabilities, and at 40 revolutions before stall, there appear to be spikes on top of the modal wave. They concluded that, "This indicates that our high-speed stage under normal stalling condition is considered a 'modal' machine, since modal instabilities dominate the pre-stall behavior with some added pip instabilities present just before stall."

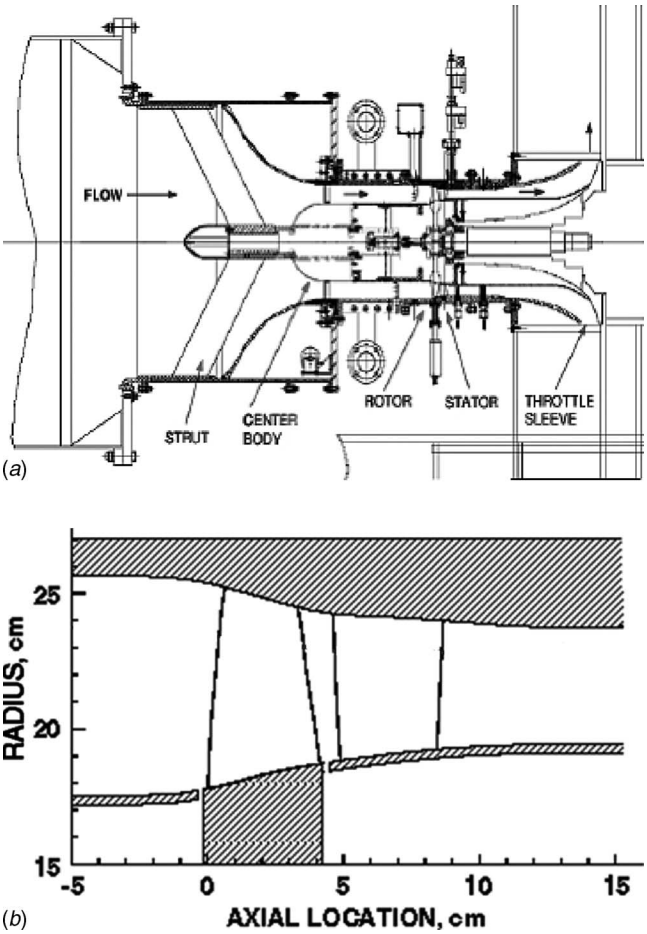

Fig. 1 NASA high-speed compressor Stage 35

In the following, we take a closer look at these experimental data. The shapes of the modal disturbances indicated in Fig. 2 resemble sinusoidal waves with a temporal period of ten rotor revolutions. The speed of the modal disturbances, as indicated by the slope of Line A, connecting the peaks of the pressure wave, is zero. This indicates that the modal disturbance is caused by axisymmetric longitudinal system disturbances. The system includes all ducting and volumes of the experimental facility. This modal disturbance is the *surge mode* that oscillates at a frequency of 10% rotor speed—equivalent to the ten rotor revolutions period it covers. Unlike a typical rotating modal wave, the surge mode does not rotate. The surge mode is a compression system wide resonance that cannot be modeled with the current simulation because the computational grid does not include the ducting of the test facility, which is quite substantial, as shown in Fig. 1.

As the compressor throttles closer to stall at about ten revolutions before stall, there is a secondary disturbance, much like a spike in the time scale of Fig. 2. Looking more closely, this secondary disturbance covers a circumferential distance of one rotor circumference, as indicated in the enlarged image. It sits on top of

Table 1 Design parameters of Stage 35

Rotor rpm at 100% speed	17,188.7
Tip speed (m/s)	454.456
Hub/tip radius	0.7
Rotor aspect ratio	1.19
Stator aspect ratio	1.26
Number of rotor blades	36
Number of stator blades	46

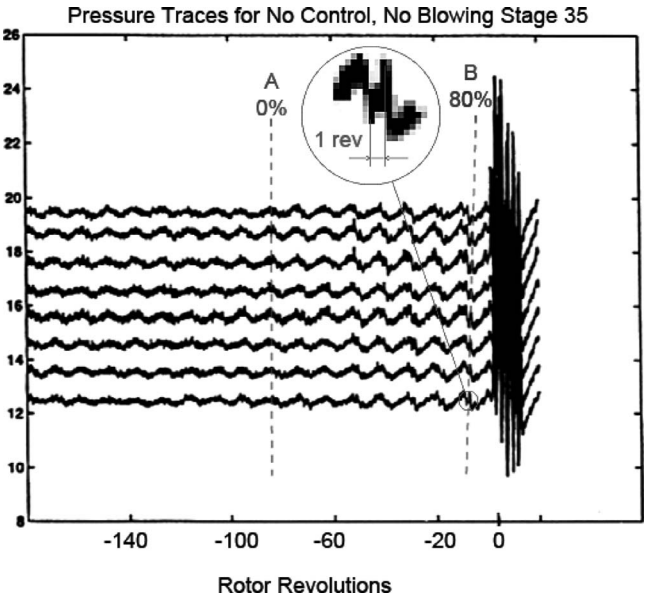

Fig. 2 Experiment pressure traces for clean inlet, 85% design speed, Stage 35, Bright et al. [17]

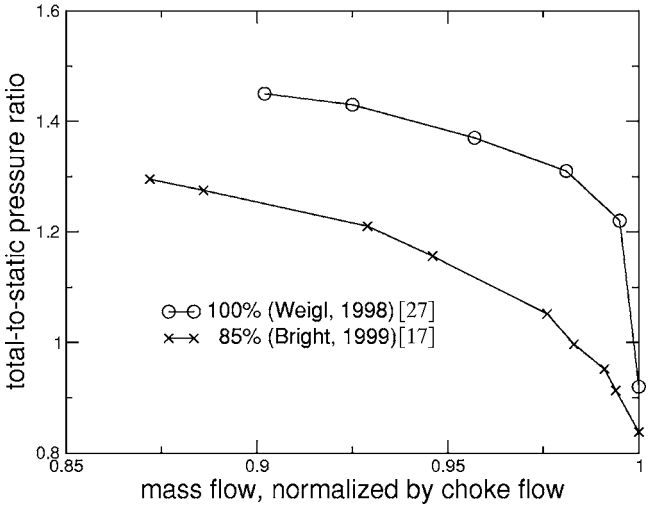

Fig. 3 Comparison of characteristics at 85%, Bright et al. [17], and 100%, Weigl et al. [27], speeds, Stage 35

the surge mode and rotates around the annulus at about 80% rotor speed, indicated by Line B. Because the length scale of this disturbance is the entire annulus, which is much larger than that of a typical spike, it is classified as a mode. For discussions in the rest of the paper, this *rotating long-length disturbance* is also referred to as a *rotating modal disturbance*. This long-length disturbance is followed by the eventual flow breakdown. Due to the picture quality, we are unable to discern the transition between the start of the rotating long-length disturbance and the final breakdown. The long-length disturbance has a length scale of *one* rotor circumference. The rotating long-length disturbance, because of its length scale, can only be resolved by a full-annulus simulation.

The simulation reported in this work is part of an overall effort to examine steady tip injection stall flow control for Stage 35 at design speed with the clean inlet. As such, the simulation was conducted at design speed. To our knowledge, there are no pressure trace data available at design speed as that shown in Fig. 2. Therefore, we will use the 85% speed case to compare with the simulated results. While the speeds are different, the two cases are both transonic compressors and share common features as we explore the flow behavior prior to stall. The experimental characteristics at 85% and 100% speeds are compared in Fig. 3. Both cases stall at the peak of static pressure rise. More importantly is that their slopes near stall are similar. These similarities justify the use of the 85% speed case for comparison.

Numerical Methodology

TURBO is a physics-based simulation tool for multistage turbomachinery. The solver computes the fluid conservation laws without ad hoc modeling of any flow phenomenon other than models required for turbulence. This code solves the unsteady Reynolds-averaged Navier–Stokes equations and a decoupled k-ε turbulence model. The code is implemented in a portable, scalable form for distributed-memory parallel computers using message passing interface (MPI). The parallel implementation employs domain decomposition and supports general multiblock grids with arbitrary grid-block connectivity. The solution algorithm is a Newton iterative implicit time-accurate scheme with characteristics-based finite-volume spatial discretization. The Newton subiterations are solved using a concurrent block-Jacobi symmetric Gauss–Seidel (BJ-SGS) relaxation scheme. Because all of the fundamental fluid mechanics are computed, the code is capable of capturing the nonlinear characteristics of the flow fields of interest. With the actual modeling of blade rows in relative motion, this code is capable of computing the unsteady interactions between blade rows. Details of the flow solver can be found from Chen and Whitfield [18]. The approach to parallelization for large-scale, complex problems is discussed by Chen and Briley [19]. In the following, we discuss several issues applied to the code in the simulation of rotating stall.

Full Compressor Stage Simulation. The intent to simulate the inception and maturation of long-wavelength circumferential modes, with wave numbers as low as unity, requires full-annulus simulations. A time-accurate sliding interface (Chen and Barter [20]) is implemented, in which pressure waves in all directions (axial, radial, and circumferential) are passed unaltered between the rotor and the stator. This attribute is necessary to examine the temporal and spatial responses associated with blade row interaction during stall inception.

Inlet Boundary Condition. An isentropic inlet condition (Chen and Whitfield [18]) is applied, where the spanwise total condition is prescribed. This boundary condition preserves the upstream total conditions at test facility level but can potentially reflect outgoing pressure waves back to the computational domain.

Exit Boundary Condition. The traditional choice of exit boundary for stable flow is the radial equilibrium condition. This boundary condition uses a preset exit static pressure. In near-stall or during-stall conditions, compressor pressure rise drops and a preset exit pressure cannot match the pressure drop. In this study, we relieve the situation by the use of a "choked" throttle model that specifies corrected mass flow at the exit. This boundary condition allows variation of exit static pressure to match the compressor exit mass corrected to the exit total condition.

Tip Clearance Model. The tip gap was modeled by the tip clearance model of Kirtley [21]. This model ensures the conservation of mass and momentum through the tip gap without the need of a tip clearance grid. A gridding strategy suggested by Van Zante et al. [22] is adopted in this study where ten points are placed in the tip gap region. Although the detailed physics of the development of the leakage vortex are not captured, the tip clearance model was considered adequate for predicting the first order effects of the leakage vortex strength, extent, and direction (Chima [23]).

Gridding. This compressor stage consists of 36 rotor blades

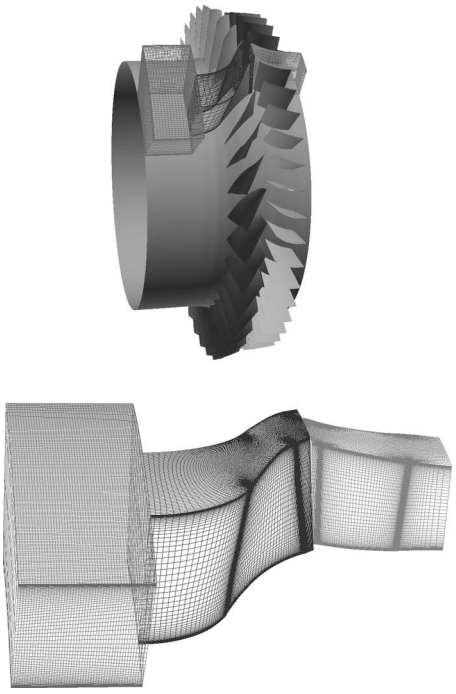

Fig. 4 Three-blade-row grid model for the Stage 35 simulation

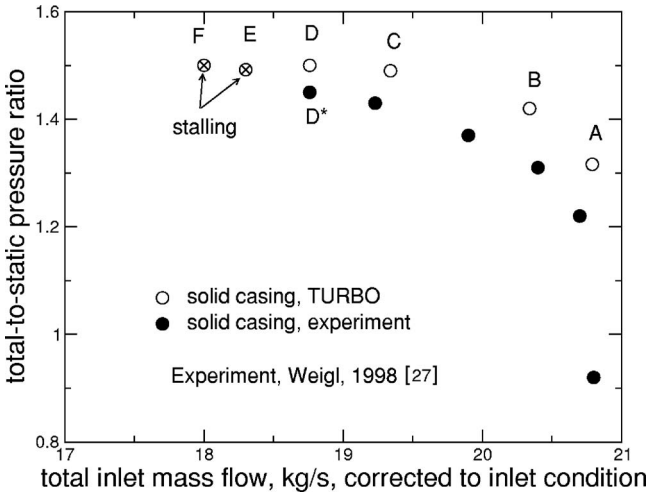

Fig. 5 Stage 35 computed and measured speedlines, design speed

and 46 stator blades. For the purpose of conducting simulations with tip injectors in another effort, we built a three-blade-row grid as shown in Fig. 4. The injector row has 12 injectors (not activated in this study) that are equally spaced in the circumferential direction. The grid size of the rotor is 151(x), 71(r), and 56(θ) with 81(x) and 61(r) points on the blade. The grid size of the stator is 141(x), 71(r), and 79(θ) with 81(x) and 53(r) points on the blade. The rotor tip clearance is 1% of rotor tip chord. The grids are replicated around the annulus to generate a full-annulus grid with a total of 67×10^6 grid points. The grid is then partitioned into 328 blocks. The simulations were run on an IBM P4 cluster at NAVO MSRC using 328 CPUs with 24 h (wall clock) computation time for one rotor revolution. In the simulation of the development of rotating stall, ten revolutions were needed. Ideally, each operating point should be run at least ten revolutions to ensure convergence, especially for points close to stall. The time for each speedline would then be 0.5×10^6 CPU hours (six operating points).

Constrained by the computational resources for the full-annulus simulations, very short upstream and downstream computational domains were used here. This choice prompts two caveats: (1) The exclusion of the test facility volume effect prevents the modeling of the surge mode. Any modal activity showing up in the simulation should be a result of the compound effect of the blades (both rotor and stator if the interaction of the two matters) and the limited volume effect present in the ducting of the current grid. (2) Limiting the axial extent of the computational domain can potentially disrupt long-length modes due to the reflective inlet boundary. Because pressure waves (with length λ) decay $e^{-L/\lambda}$ through a distance L, it is preferred to place the inlet boundary away from the rotor so that pressure waves, especially with long wavelengths, decay sufficiently before reaching the inlet. Typically, the modal instability shows up hundreds of revolutions prior to stall. Complete simulation of the evolution of such modal instability is beyond the computational resources available in this study. Our intent, therefore, is to examine the development of the modal disturbances as they first emerge before reaching the inlet rather than the complete resolution of the modal stall process. In this aspect, a shorter upstream domain (2.5 rotor chords) is justified.

Results and Discussions

The difference of the throttling processes in the simulation and the experiment is that in the simulation, the exit boundary condition is changed in discrete steps, while in the experiment, the compressor transitioned to stall through a continuous throttling maneuver. In this simulation, a new throttle setting restarts from the solution of a previous throttle setting. Due to computational resources, each throttle setting was only run for a few revolutions before moving to the next. Generally, it was sufficient to reach convergence within four revolutions while away from stall. As stall was approached, more (six or more) revolutions were required to assure convergence.

Stage Characteristics. The computed and experimental characteristics (speedlines) are shown in Fig. 5. The data used in this figure are the ratio of exit static pressure to inlet total pressure versus mass rate corrected to inlet total condition. The computed speedline is generated by incrementally closing the throttle setting (decreasing exit corrected mass flow) from A to F. The overall shape of the computed characteristic before stall is similar to the experimental data, so is the slope of the characteristic near the peak pressure (throttle Point D). Since the slope of the compressor characteristic correlates with the type of stall inception, we consider the simulation reasonable to capture the stall inception mechanisms.

Point D in Fig. 5 is the last stable throttle setting. Points E and F both restart from Point D and develop into a rotating stall. In both cases, the exit pressure changes from the peak at D into a transitional peak and then drops to a much lower level during rotating stall, as shown in Fig. 6(a). This demonstrates the throttling effect of the corrected mass exit boundary condition by allowing the exit pressure to vary as the flow condition changes. The pressure ratios shown in Fig. 5 for E and F are the transitional peak pressures before entering rotating stall. Point D^* is the approximate stall point from the experiment. The actual simulated stall point should occur between D and E. The actual stall point depends on many issues, such as tip clearance height, deviation of real blade geometry from designed geometry, as well as the type of turbulence modeling in the numerical simulation. These details may not be correctly represented in this simulation. Even though the exact stall point is important, for the intent of this study, the simulation is considered adequate to examine the general physical trends leading to stall.

In the following sections, we first present the entire evolution of the rotating stall as the throttle setting changes from D to F. This

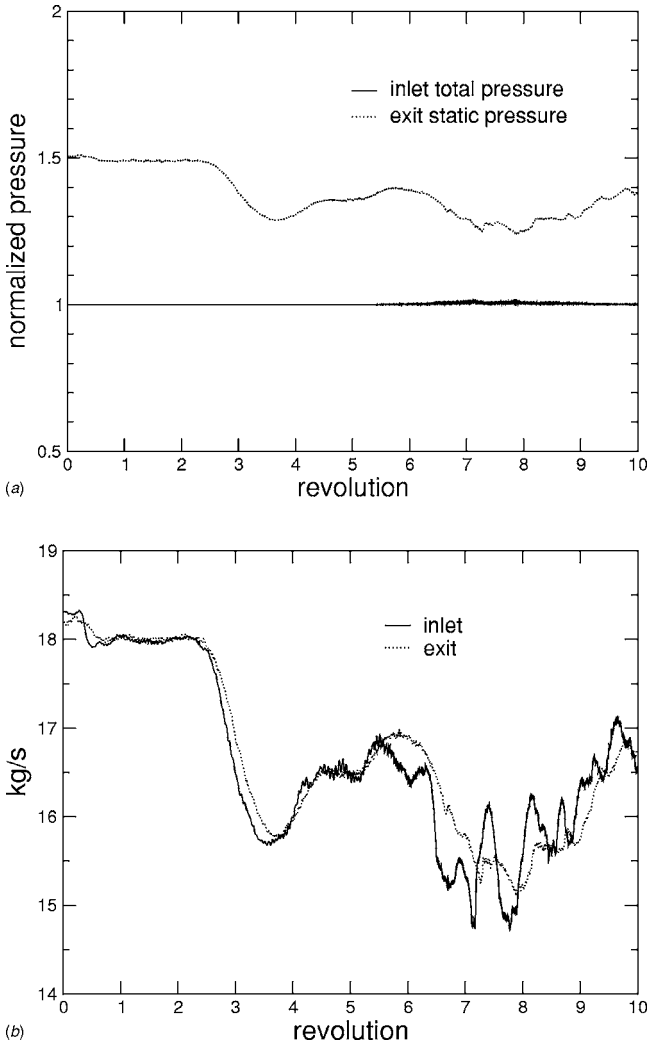

Fig. 6 Pressure and mass variation during rotating stall at throttle Setting F: (*a*) Pressure (*b*) mass flow

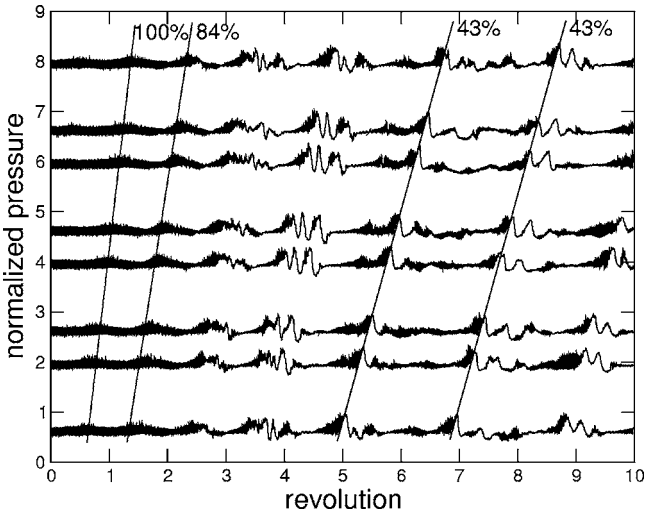

Fig. 7 Time history of static pressure variation at eight locations around the annulus located 44% chord ahead of the rotor of Stage 35, throttling Setting F

is followed by a closer examination of the prestall flow development from D to E, with E being closer to the stable point D.

Evolution of the Rotating Stall. This result was reported by Chen et al. [13] and is outlined here for completeness. The rotating stall was captured by the time variation of static pressure at eight pressure transducers circumferentially spaced upstream of the rotor. The probes are located 44% chord upstream of the rotor leading edge at 98% span. The circumferential locations are 10 deg, 70 deg, 100 deg, 160 deg, 190 deg, 250 deg, 280 deg, and 340 deg. The history of pressure variations are shown in Fig. 7, in which the pressure levels are offset by the probe circumferential locations. Because the volume effect is not modeled in the simulation, the pressure disturbance of Fig. 7 should be viewed as a filtered version of Fig. 2 by removing the surge mode oscillations.

Small, periodic pressure variations caused by the rotor blade passing, as indicated by the thickness of the curves, are present in all curves of Fig. 7. A smooth disturbance is visible at $t=0.7T$ (T=time for one rotor revolution) traveling at full rotor speed. This disturbance, analyzed in further detail later, has a length scale of one rotor circumference, thus is classified as a modal disturbance. The rotating modal disturbance continues to grow in magnitude but the speed slows to 84% rotor speed in approximately one revolution. After $2T$, it transforms into several spike disturbances around the annulus, each with a smaller length scale of a few blade passages. The spike disturbances then grow in magnitude and slow down to 43% in four revolutions. Inlet and exit mass flow histories during the same period are shown in Fig. 6(*b*), in which the mass flow remains relatively flat in the first two revolutions at 18 kg/s before it drops sharply and sustains large variations of 14% of the peak mass flow.

In Figs. 8 and 9, the entropy on a surface of revolution near the casing is shown at two instants in time. The full-annulus surface is illustrated by two half-annulus surfaces. At $t=3.8T$, Fig. 8, the early phase of the stall inception, three separate high entropy (red color) regions can be seen, with the axial extent covering from one chord upstream to aft of the stator leading edges. The radial extent of the stall cell is shown in the axial cut plane at 16% chord before the rotor, where the high entropy region shows the stall cell extending about 30% span from the casing. At $t=10T$, Fig. 9, the stall cell evolves into the final stage as its rotating speed becomes stabilized. The three-cell stall has merged into a single-cell stall with the axial extent covering all the way from the inlet of the computation domain to aft of the stator trailing edge. The radial extent of the stall cell has now extended about 70% span from casing.

The evolution of the simulated rotating stall cell is similar to the spike stall inception mechanism commonly observed in that localized, three-dimensional pockets of instability in multiple rotor passages break up to form the initial phase of a rotating stall cell, usually with several small-sized stall cells. These small stall cells move fast at the beginning and then merge into a single rotating stall cell within a few revolutions before slowing down to about half of the rotor speed as the rotating stall becomes fully developed.

In the previous section, we gave a brief description of the overall evolution of the rotating stall using throttle Setting F. In the following sections, we will examine the process that leads to the initial flow breakdown, i.e., the stall inception process. Restarting from the stable solution of D, the simulation was repeated with throttle Setting E, the mass flow history during the transition from D to E is shown in Fig. 10. The simulation shows that after four revolutions from restart, the mass flow starts to decrease, leading to the rotating stall. Three time stamps marked E1 ($1.7T$), E2 ($3.2T$), and E3 ($4.3T$) will be referenced in the following discussions.

Development of Long-Length Disturbance. Both experimental (Spakovszky et al. [24] and Suder et al. [25]) and computational studies (Chen et al. [13], Davis and Yao [9]) indicate that

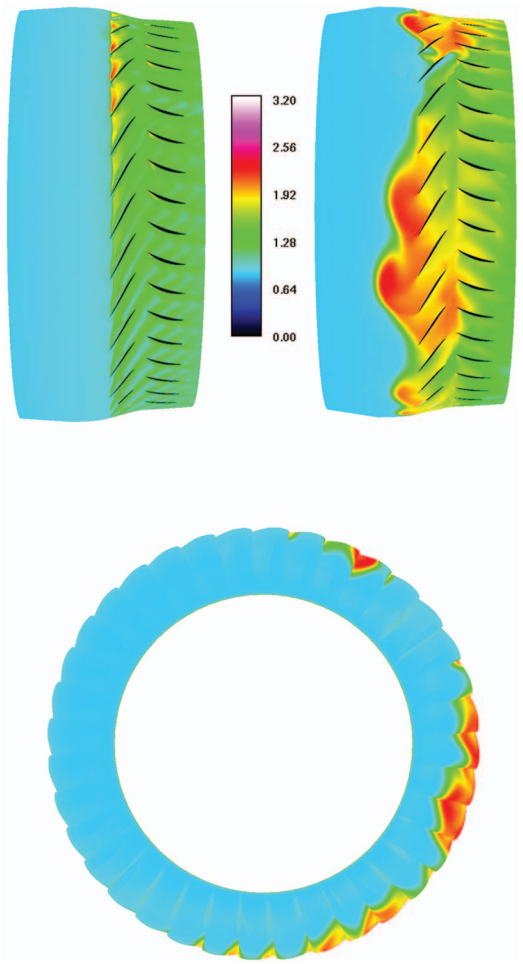

Fig. 8 Entropy of Stage 35 during stall inception, $t=3.8T$: Left half annulus and right half annulus, 16% chord upstream of rotor leading edge

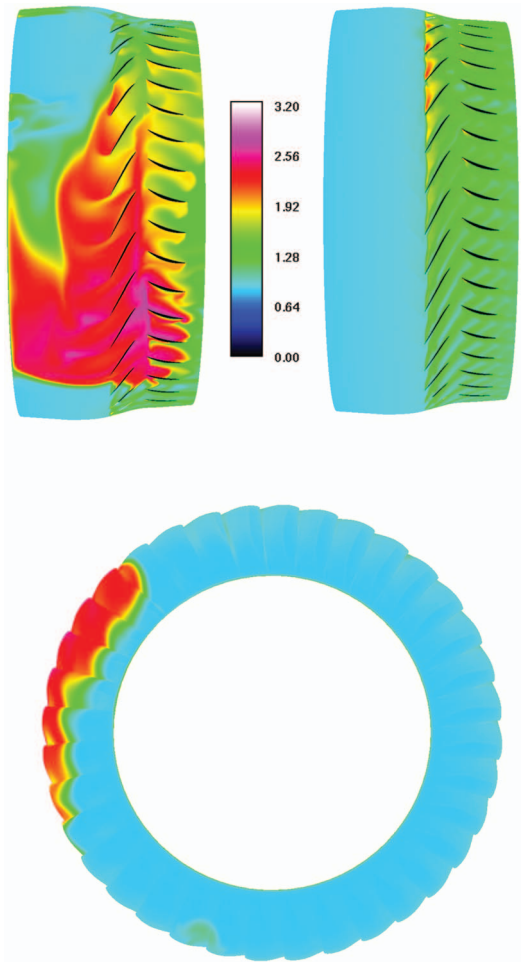

Fig. 9 Entropy of Stage 35 during stall inception, $t=10T$: Left half annulus and right half annulus, 16% chord upstream of rotor leading edge

the rotating stall of this compressor initiates in the rotor tip region, so the analysis will focus on the rotor tip. Instantaneous pressure profiles around the annulus near the rotor tip leading edge are shown in Fig. 11. The three curves correspond to different phases at throttle Settings D and E during the transition from stable operation to stall (Fig. 10). Phase 1 is the last stable point before stall, which will be used as the base line for comparison. Phases 2 and 3 are the same throttle Setting E, but at two different instants: one before stall (Time E1) and the other at the beginning of stall (Time E2). Spatial fast Fourier transforms (FFTs) of the pressure profile are shown in Fig. 12. The most dominant harmonic is the 36th mode (its magnitude is at least one order of magnitude larger than those of others), which corresponds to the number of rotor blades. This disturbance is caused by the periodic flow features between blades and thus has the length scale associated with the rotor blade pitch. Not shown here is the strength of the 46th mode, which is negligible. This indicates that the influence of the stator on the potential field at rotor leading edge can be ignored. Therefore we will focus the study only on the rotor.

Modal disturbances, if any, should exist in the low harmonics with longer wavelengths that are on the order of the rotor circumference. At Phase 1 (D), only the 36th mode prevails. This indicates that when away from stall, the only disturbance to the otherwise uniform annulus flow is that from the periodic rotor passing and there is no modal activity. At Phase 2 (Time E1), the early phase of the rotating stall, there exists an identifiable 1st mode along with the 36th mode. There are also weaker but identifiable modes between the 1st and 36th modes. As the simulation proceeds, bringing the compressor even closer to stall at Phase 3 (Time E2), the magnitude of the first mode increases even more. The magnitudes of the modes in between remain relatively similar to those in the previous two phases but fluctuate over the spectrum. The only mode that grows persistently during the prestall phase is the first mode. This disturbance rotates at 100% rotor speed. This observation is the same as that of throttle Setting F, where the speed of rotating mode is indicated in the pressure history of Fig. 7. This finding is similar to the experiment (see Fig. 2) in that the one rotor circumference disturbance, which sits on top of the surge mode (not modeled in this simulation), starts to rotate at 80% rotor speed right before stall. It suggests perhaps that the simulation is adequately modeling the one rotor circumference modal disturbance before the compressor enters rotating stall.

A possible explanation of the origin of the first mode can be derived from the following observations: (1) While the grid in our simulation does not include the complete ducting system, it does include the limited ducting that contains the rotor and the stator. (2) The speed of the rotating mode is 100% rotor speed; in other words, the first mode is fixed to the rotor. This makes it likely that the disturbance is associated with the rotor. The two observations suggest that the first mode may originate from a compound effect of the rotor blades and the limited volume effect present in the ducting of the current grid.

Development of Mode and Spike. To better understand the development of the first mode and the spike disturbance, we focus

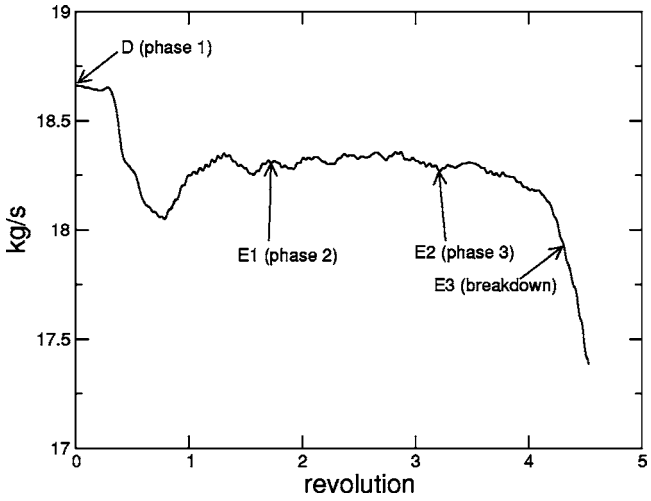

Fig. 10 Mass flow history at throttle Setting E

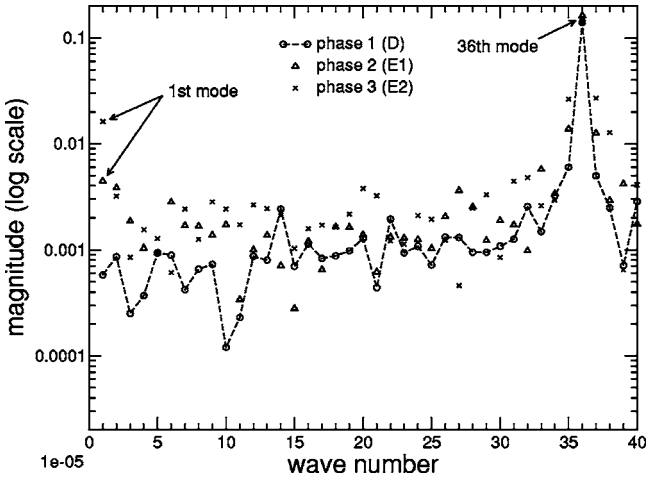

Fig. 12 FFT of Fig. 11

on the evolution of the flow during the transient right before stall. Since stall is likely to be associated with the reverse flow (negative axial flow), we will monitor the development of the negative axial velocity of the flow during the transition. Figures 13(*a*)–13(*c*) illustrate the axial velocity of the stage at three radial cut planes at the three time instants E1, E2, and E3 during the transient. The three cut planes are located at 4 clearance heights (4ε) below casing (Cut plane 1), 1.5 clearance heights (1.5ε) below casing (Cut plane 2), and 0.5 clearance heights (0.5ε) below casing (Cut plane 3). Figure 13(*d*) illustrates the front views of Cut plane 3 at the three time instants. The contours of the axial velocity have been truncated so that only the negative velocity has a color. All positive velocities are colored white.

At Time E1, Fig. 13(*a*), about 2.5 revolutions before breakdown, the reverse flow is seen in all rotor passages with a radial coverage of at least four clearance heights below the casing, as indicated by the reverse flow being visible on all cut planes. The rotor reverse flow is formed by the tip clearance vortex flow, which will be explained in detail later. The boundary and magnitude of the reverse flow region depicts the boundary and the strength of the tip vortex. The patterns of the reverse flow are not the same in every passage, with the reverse flow zone larger on the back side of the view (210 deg). This can be readily seen on Cut planes 1 and 2. The overall shape of rotor reverse flow corresponds well with the harmonics of Fig. 12 in that the 1st mode coexists with the 36th mode. The speed of the 1st mode is the same as that of the 36th mode, both rotate at the rotor speed. The flow at this phase has already shown the instability.

At Time E2, by comparing the front view of Cut plane 3 at Times E1 and E2 [Fig. 13(*d*)], we see that the front boundary of the reverse flow moves forward and becomes perpendicular to the axial direction. The magnitude of the negative velocity at Time E2 is also higher than that at Time E1 as is shown by more green spots at Time E2. This is consistent with the short-length stall inception mechanism described by Hoying et al. [7] that spike stall initiates when the tip clearance vortex trajectories align perpendicularly to the axial direction. The larger reverse flow zone now rotates to the front side of the view (0 deg), Fig. 13(*b*), better seen on Cut planes 1 and 2. Also seen on the two cut planes is the appearance of reverse flow in the stator. Different from the reverse flow in the rotor, which is caused by tip clearance vortex, the stator reverse flow is caused by suction surface flow separation.

At Time E3, 1.1 revolutions after Time E2, the flow formally enters the rotating stall. A zone of extended reverse flow covering five rotor passages can now be seen in the front view of Cut plane 3 (330 deg) in Figs. 13(*c*) and 13(*d*). This zone sits in the middle of the less extensive reverse flow characterized by the green colored tip clearance flow on Cut plane 3. This less extensive reverse flow correlates with the first mode. The five-passage reverse flow zone initiates a spikelike disturbance on top of the first mode and finally leads to the rotating stall.

Further analysis of the simulation also indicates the correlation between the first mode disturbance of axial momentum and the appearance of spike. The circumferential profile of the axial momentum near the rotor tip leading edge is low-pass filtered to remove high-frequency noise so only the first mode stays. Figure 14 shows the results at Times E1, E2, and E3. The magnitude of the first mode disturbance grows from E1 to E3 as it rotates around the annulus. The locations of the trough of the waves (marked in Fig. 14) are where the flow has the lowest axial momentum. These locations match the regions of the larger reverse flows in all three cut planes mentioned previously. This is consistent with the observation of Day [5] that spikes can grow out of the trough of the axial velocity modal waves if critical incidence is reached.

As we pointed out before, it is difficult to discern the actual transition from the rotating modal wave to the start of the rotating stall in Fig. 2. The simulation provides the details to complement the experiment. It is demonstrated here that a spike of five passages long does occur. It evolves smoothly out of the rotating mode and eventually leads to the breakdown (rotating stall).

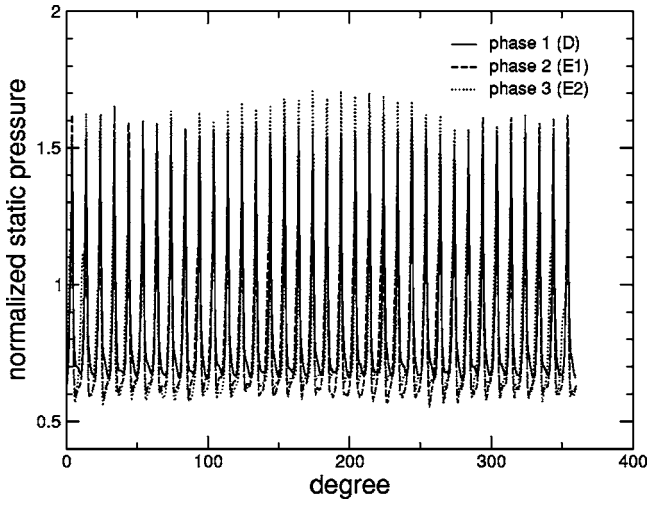

Fig. 11 Instantaneous pressure profile at rotor tip

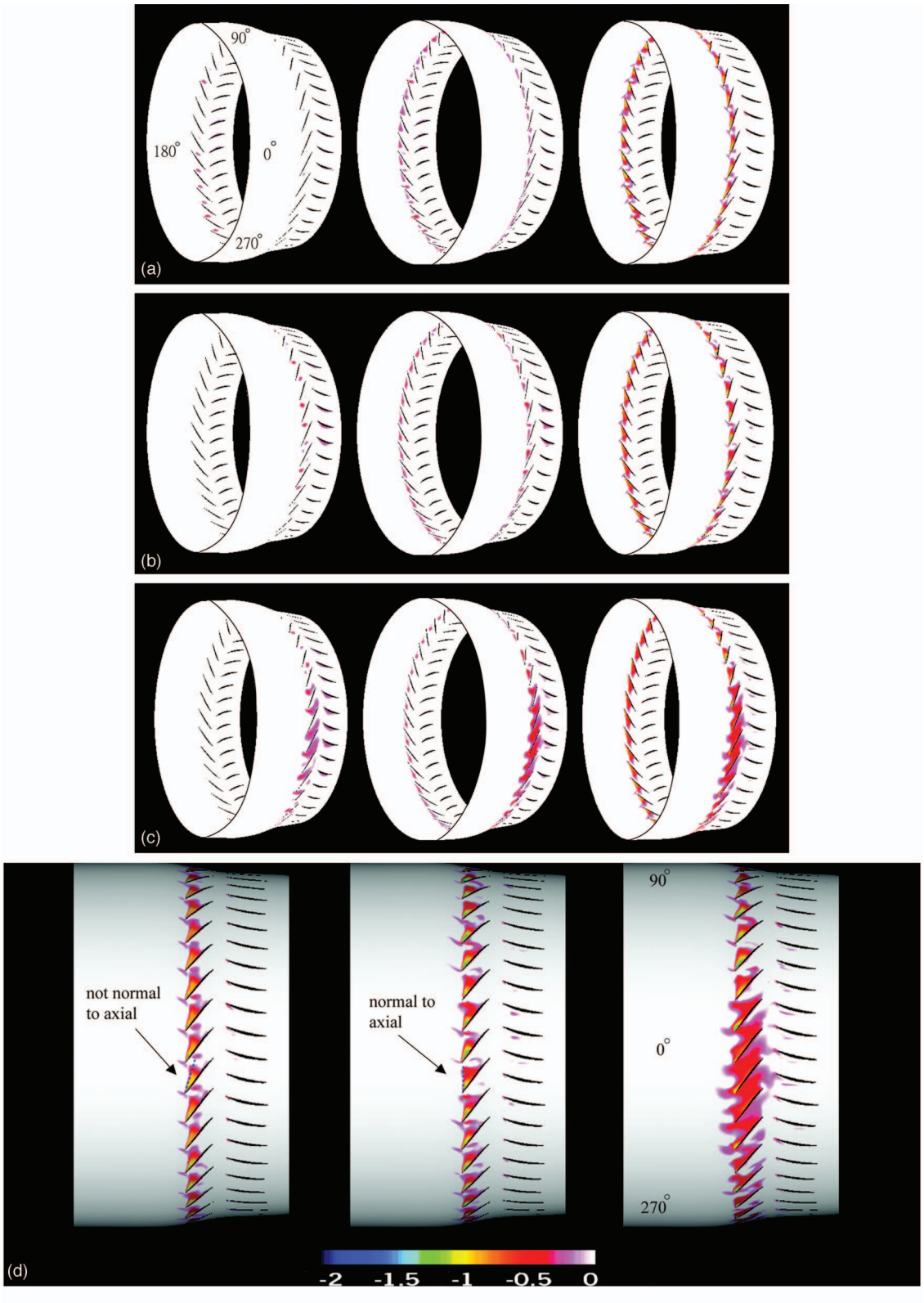

Fig. 13 Negative axial velocity at three cut planes, three time instants: (*a*) Time E1 (2.5*T* before rotating stall), (*b*) Time E2 (beginning of rotating stall), and (c) Time E3 (during rotating stall); Left to right, cut plane 1 (4ε), cut plane 2 (1.5ε), cut plane 3 (0.5ε). (*d*) Left to right, front views of cut-plane 3 (0.5ε) at three time instants, E1, E2, and E3, negative axial velocity.

Interaction of Shock and Tip Clearance Flow. Interaction between the tip clearance flow and shock in transonic compressor has been cited as one of the initiators of spike disturbance. As noted by Day [5], short-length spikes can be viewed as embryonic stall cells with flow breakdown in local regions; it is a 3D phenomenon. Computational simulations using a single blade passage

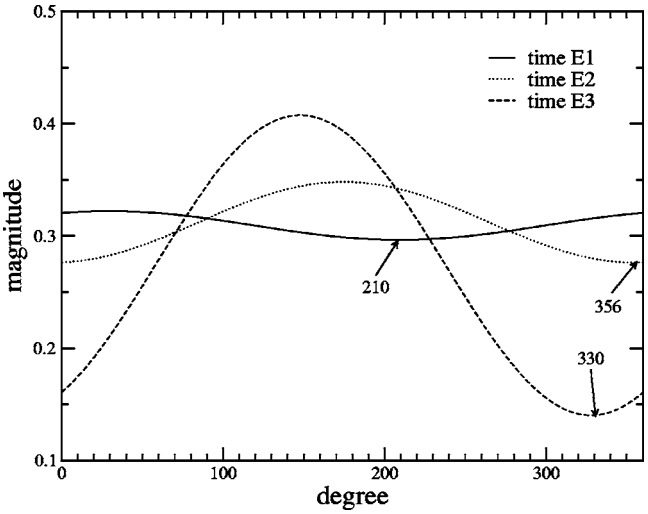

Fig. 14 First mode disturbances of axial momentum at rotor tip

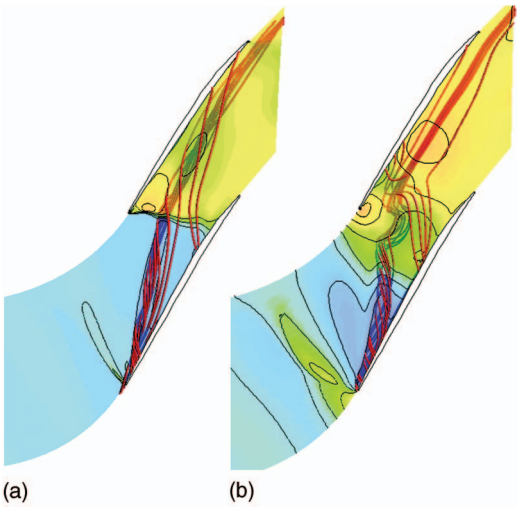

Fig. 16 Streamlines forming the tip clearance vortex: (*a*) Stable condition and (*b*) near-stall condition (Time E1)

to study the effect of the tip clearance flow on the onset of stall were reported by Adamczyk et al. [26]. One generally agreed conclusion is that the tip clearance vortex moves forward from stable to stall condition. Using vortex kinematics arguments, Hoying et al. [7] developed a criterion for stall inception when the trajectory of the tip clearance vortex becomes perpendicular to the axial direction. Vo et al. [8] also demonstrated that stall inception is most likely accompanied by the forward spillage of tip clearance vortex. One might ask the following: How does the shock interact with the tip clearance flow? Does the shock directly cause flow separation that may contribute to the stall inception?

To answer these questions, we take a closer look at the flow within the rotor passage. A comparison of pressure contours near the casing between the stable and near-stall (Time E1) conditions is made in Fig. 15. In the stable condition, the pressure fields in the two passages shown are almost identical. There exists a distinguishable attached oblique passage shock, which originates from the leading edge of the rotor blade and extends across the passage to 80% chord on the suction surface of the adjacent blade. At Time E1, the pressure fields between passages are no longer identical. Even though the flow structure is not identical among passages, there is still similarity between them before the flow breakdown. We will discuss the common features that are generic for the rotor passages before stall. Examining the pressure field at Time E1, we see that the single attached oblique shock now changes to a more complicated dual-shock system: A strong detached shock followed by a weaker secondary shock. The strong detached shock, together with the stagnant flow around the leading edge, creates a high pressure region near the leading edge of the pressure surface. The pressure outside this area is relatively low until aft of the secondary shock where the pressure level rises again to fill uniformly between the blades.

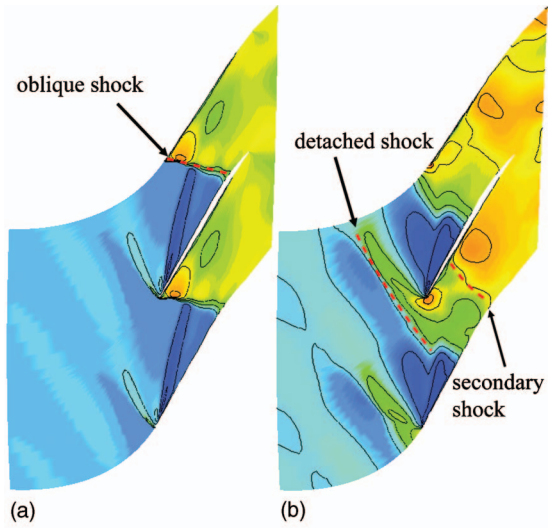

Fig. 15 Pressure contour near casing: (*a*) Stable condition and (*b*) near-stall condition (Time E1)

Streamlines forming the tip clearance vortex for both stable and near-stall (Time E1) conditions are shown in Fig. 16. The pressure contour near the casing is overlaid in the background to help the discussion. First, take a look at the stable condition. Only the forward 15% portion of the tip clearance flow emerges to form the core of the tip clearance vortex. The trajectory of the tip clearance vortex is not perpendicular to the axial direction. The oblique shock intersecting the vortex only slightly alters the shape of the vortex. The vortex moves away from the pressure surface of the adjacent blade without impinging it.

At the near-stall condition (Time E1), Fig. 16(*b*), the core vortex, again formed by the forward 15% of the tip clearance flow, now moves forward. The center portion of the vortex trajectory becomes perpendicular to the axial direction. This trend follows well with the stall inception criterion of Hoying et al. [7]. However, the shape of the vortex trajectory is first pushed backward by the high pressure near the pressure surface leading edge and then forward by the high pressure behind the secondary shock as it proceeds downstream. This distortion of the vortex trajectory is caused by the dual-shock system. The criterion of Hoying et al. [7], developed for low-speed machines, still holds for areas not affected by the dual shock. It is unclear whether or not the distorted vortex can accelerate the flow breakdown, but it is clear that the distortion occurs as the flow is close to stall with the existence of the dual shock.

Flow is likely to separate due to the shock-boundary layer interaction, in which the low momentum flow in the boundary layer is subjected to the sudden pressure rise across the shock. Thus, it is of interest to examine whether shock-induced flow separations occur in the simulation. There are two possible locations for flow separation in the rotor passage: One is on the suction surface and the other is on the casing surface. By examining the streamlines in Fig. 16, we rule out the suction surface separation. To search for the casing separation, the velocity vector in the meridional view is examined. Figure 17(*a*) shows such a plane 30% pitch off the

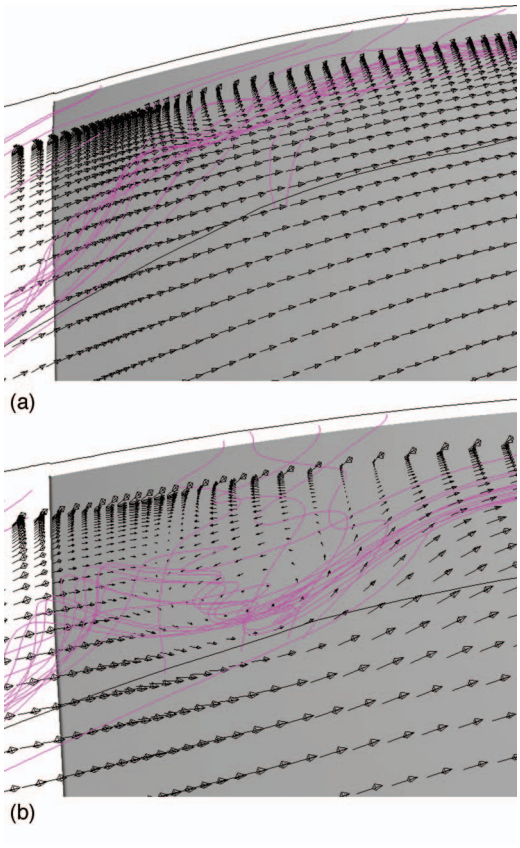

Fig. 17 Velocity vector on a meridional plane 30% pitch off pressure surface: (*a*) Stable condition and (*b*) near-stall condition (Time E1)

pressure surface. There is no observable reverse flow in this view. This indicates that the vortex moves straight downstream and that the flow remains attached to the casing. At Time E1, the reverse flow associated with the distorted vortex can be seen in Fig. 17(*b*). The velocity vector shows that the flow reversal occurs beneath the casing and is caused by the organized spiraling fluids of the distorted vortex. There is no indication of casing separation at this instant. The cross section of the vortex, however, is larger than the stable condition. This also shows that the negative axial velocity of the rotor flow shown in Fig. 13 is caused by the spiraling fluids of the tip clearance vortex and has no association with casing or blade separation. With the above observations, we conclude that there is no shock-induced separation in this during the stall inception.

As the compressor proceeds more into stall between Times E2 and E3, the flow breaks down, i.e., the mass flow rate through the compressor is declines. The reverse flow in a few passages combines to form the large blockage as shown in Figs. 13(*b*) and 13(*c*), which in turn expels flow to adjacent blades. The blockage creates the spike-type disturbance over a few passages. The expelled flow entering the adjacent blade passages brings in extra axial momentum to the casing areas of these passages. The additional axial momentum behaves like tip injection, which reduces rotor incidence levels, relative to Time E1. The vortex shape and shock structure of two passages at Time E2 are compared in Fig. 18. Figure 18(*a*) is a passage where the spike occurs. The shape of the vortex trajectory and shock structure is similar to those at Time E1, Fig. 16(*b*), only that the vortex continues to grow and the high pressure behind the detached shock pushes the vortex backward so the trajectory moves away from being perpendicular to the axial direction. Spillage of tip clearance forward of the leading edge can be seen in Fig. 19(*a*), where it is colored by the

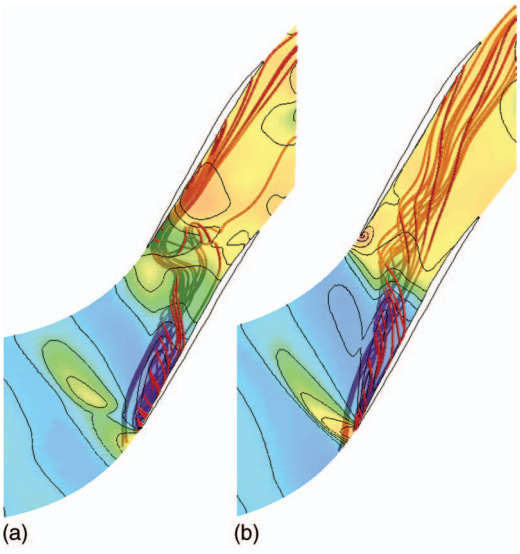

Fig. 18 Tip clearance vortex at Time E2: (*a*) Deteriorating passage and (*b*) improving passage

pink stream lines. In the passage where the flow condition improved, as shown in Fig. 18(*b*), the dual-shock system returns to a single shock and the vortex trajectory is not distorted. There is no spillage of the tip clearance flow forward of the leading edge, Fig. 19(*b*).

Simulation Summary

1. The simulation results of the high-speed axial compressor Stage 35 provide evidence that the current numerical procedure may be adequate for predicting the onset of flow instabilities and their subsequent growth into a fully developed rotating stall. The simulation results clearly show a full-annulus first mode disturbance starting to travel at 100% rotor speed at the peak of the pressure rise transitioning to a spike disturbance traveling at 84%

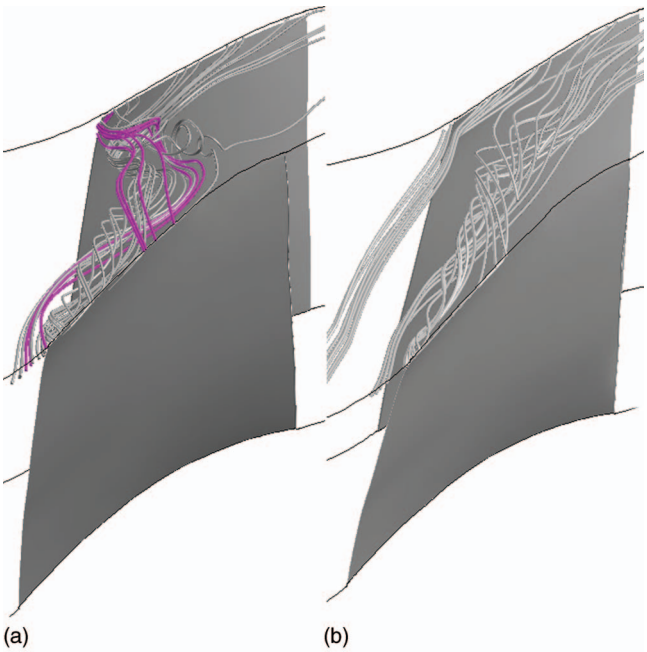

Fig. 19 Tip clearance flow showing spillage over rotor leading edge at Time E2 (*a*) spillage in deteriorating passage and (*b*) no spillage in improving passage

rotor speed. This spike disturbance then splits into multiple stall cells while their speeds reduce. Finally the multiple stall cells coalesce into a large single stall cell that rotates at 43% of rotor speed when fully developed. This simulation models the natural growth of the stall process without the use of an artificial inlet distortion.

2. As the simulation is throttled to stall, small amplitude long-length waves of 1st mode and high-order modes between the 1st and the 36th can be discerned. The magnitudes of the high-order modes fluctuate but do not grow much during the transition to stall. The first mode wave, however, persistently grows before breakdown. A short-length disturbance covering five rotor passages bursts into a spike like disturbance during the breakdown. This spike disturbance then grows into a rotating stall.

3. The computed first mode disturbance has a length scale closely resembling the one rotor circumference disturbance prior to stall in the experiment. The computed speed of the first mode disturbance (100% rotor speed) is also similar to the measured speed (80% rotor speed) of the first mode disturbance from the experiment, estimated from the results of Fig. 2. The difference is within the resolution of the picture quality of the published data.

4. The first mode of the axial momentum correlates well with the appearance of the growing reverse flow. The trough of the axial momentum matches the region of the larger reverse flow that leads to the birth of the initial spike.

5. The interaction of the shock and tip clearance vortex is examined. As the compressor approaches stall, the trajectory of the tip clearance vortex moves forward to become perpendicular to the axial direction. The shock system, in the meantime, also moves forward, changing from an attached oblique single shock to a dual shock. The pressure field of the dual-shock system distorts the trajectory of the tip clearance vortex, creating a large reverse flow region in the distorted vortex. The reverse flow in the rotor is the outward tip clearance vortex as no shock-induced casing or blade separation is found.

6. During the flow breakdown, spillage of the tip clearance flow forward of the rotor leading edge is found in several passages, where the flow condition is deteriorating. A large blockage region is formed in the deteriorating passages; this in turn impels flow to enter into adjacent passages. The influx of fluid momentum in the adjacent passages improves the flow condition there.

Conclusions

The TURBO code has been applied to the 3D full-annulus simulation of a transonic compressor stage NASA Stage 35 to investigate the flow evolution prior to stall. This simulation does not include the system volume, and therefore cannot model the surge mode oscillation that arises from the test facility ducting system. With the surge mode removed, the stalling flow first takes the form of a rotating long-length (modal) disturbance; it then changes into a spike. The spike seems to grow out of the long-length disturbance and eventually leads to stall. The spike emerges when the tip clearance vortex becomes perpendicular to the axial direction and, in some passages, with forward spillage. The passage shock changes from single shock to dual shock when approaching stall. The dual shock distorts the trajectory of the vortex but does not cause flow separation that directly contributes to the stall. The simulation correlates well with the experiment data excluding the surge mode. The computational resources involved in conducting such a simulation are prohibitively large at the time and are not suitable for routine executions. While this is certainly an issue, the key point is that the simulations of this type generate qualitatively and quantitatively accurate flow field data that can support our understanding and inferences of the unsteady compressor flow field, including support and interpretation of experimental work.

Acknowledgment

The authors would like to acknowledge the invaluable discussions and technical advises from Dr. John Adamczyk, Dr. Dale Van Zante, Dr. Gerard Welch, and Dr. Tony Strazisar of NASA Glenn Research Center, and Dr. Choon Tan, Dr. Yifang Gong, and Professor Edward Greitzer of MIT Gas Turbine Laboratory. Thanks to Mr. Sean Barrows, Mr. Trevor Goerig, and Mr. Benjamin Johnson of The Ohio State University for their hard work in preparing the manuscript. The high-performance computing resources are provided by DoD Grand Challenge Project, Ohio Supercomputing Center, and IBM. Financial support comes from AVETEC, with Robert Evans Miller as project manager, and Army Research Office, with Thomas Doligalski as project manager. These supports are greatly appreciated.

References

[1] Moore, F. K., and Greitzer, E. M., 1986, "A Theory of Post-Stall Transients in Axial Compressors—Part I: Development of the Equations," ASME J. Eng. Gas Turbines Power, **108**, pp. 68–76.
[2] McDougall, N. M., 1988, "Stall Inception in Axial Compressors," Ph.D. thesis, Cambridge University, Cambridge.
[3] Garnier, V. H., Epstein, A. H., and Greitzer, E. M., 1991, "Rotating Waves as a Stall Inception Indication in Axial Compressors," ASME J. Turbomach., **113**, pp. 290–302.
[4] Camp, T. R., and Day, I. J., 1998, "Study of Spike and Modal Stall Phenomenon in a Low-Speed Axial Compressor," ASME J. Turbomach., **120**(3), pp. 393–401.
[5] Day, I. J., 1993, "Stall Inception in Axial Flow Compressors," ASME J. Turbomach., **115**, pp. 1–9.
[6] Cumpsty, N. A., 2004, *Compressor Aerodynamics*, Krieger, Malabar, FL.
[7] Hoying, D. A., Tan, C. S., Vo, H. D., and Greitzer, E. M., 1998, "Role of Blade Passage Flow Structures in Axial Compressor Rotating Stall Inception," ASME J. Turbomach., **121**, pp. 735–742.
[8] Vo, H. D., Tan, C. S., and Greitzer, E. M., 2005, "Criteria for Spike Initiated Rotating Stall," ASME Paper No. GT2005–68374.
[9] Davis, R. L., and Yao, J., 2006, "Prediction of Compressor Stage Performance From Choke Through Stall," J. Propul. Power, **22**(3), pp. 550–557.
[10] Gong, Y., Tan, C. S., Gordon, K. A., and Greitzer, E. M., 1999, "A Computational Model for Short Wavelength Stall Inception and Development in Multistage Compressors," ASME J. Turbomach., **121**, pp. 726–734.
[11] He, L., 1997, "Computational Study of Rotating-Stall Inception in Axial Compressors," J. Propul. Power, **13**(1) pp. 31–38.
[12] Saxer-Felici, H. M., Saxer, A. P., Inderbitzin, A., and Gyarmathy, G., 2000, "Numerical and Experimental Study of Rotating Stall in an Axial Compressor Stage," AIAA J., **38**(7) pp. 1132–1141.
[13] Chen, J. P., Webster, R. S., Hathaway, M. D., Herrick, G. P., and Skoch, G. J., 2006, "Numerical Simulation of Stall and Stall Control in Axial and Radial Compressors," AIAA Paper No. AIAA-2006-418.
[14] Hah, C., Bergner, J., and Schiffer, H.-P., 2006, "Short Length-Scale Rotating Stall Inception in a Transonic Axial Compressor—Criteria and Mechanisms," ASME Paper No. GT2006–90045.
[15] Hathaway, M. D., Chen, J., Webster, R., and Herrick, G. P., 2004, "Time Accurate Unsteady Simulations of the Stall Inception Process in the Compression System of a U.S. Army Helicopter Gas Turbine Engine," 2004 DoD High Performance Computing Modernization Program User's Group Conference, Williamsburg, VA, June 7–10.
[16] Reid, L., and Moore, R. D., 1978, "Performance of Single-Stage Axial-Flow Transonic Compressor with Rotor and Stator Aspect Ratios of 1.19 and 1.26, Respectively, and With Design Pressure Ratio of 1.82," NASA Technical Report No. TP-1338.
[17] Bright, M. M., Qammar, H. K., and Wang, L., 1999, "Investigation of Pre-Stall Mode and Pip Inception in High-Speed Compressors Through the Use of Correlation Integral," ASME J. Turbomach., **121**, pp. 743–750.
[18] Chen, J. P., and Whitfield, D. L., 1993, "Navier-Stokes Calculations for the Unsteady Flowfield of Turbomachinery," AIAA Paper No. AIAA-93–0676.
[19] Chen, J. P., and Briley, W. R., 2001, "A Parallel Flow Solver for Unsteady Multiple Blade Row Turbomachinery Simulations," ASME Paper No. GT-2001-348.
[20] Chen, J. P., and Barter, J., "Comparison of Time-Accurate Calculations for the Unsteady Interaction in Turbomachinery Stage," AIAA Paper No. AIAA-98-3293.
[21] Kirtley, K. R., Beach, T. A., and Adamczyk, J. J., 1990, "Numerical Analysis of Secondary Flow in a Two-Stage Turbine," AIAA Paper No. AIAA-90–2356.
[22] Van Zante, D. E., Strazisar, A. J., Wood, J. R., Hathaway, M. D., and Okiishi, T. H., 2000, "Recommendations for Achieving Accurate Numerical Simulation

of Tip Clearance Flows in Transonic Compressor Rotors," ASME J. Turbomach., **122**, pp. 733–742.
[23] Chima, R. V., 1998, "Calculation of Tip Clearance Effects in a Transonic Compressor Rotor," ASME J. Turbomach., **120**, pp. 131–140.
[24] Spakovszky, Z. S., Weigl, H. J., Paduano, J. J., van Schalkwyk, C. M., Suder, K. L., and Bright, M. M., 1999, "Rotating Stall Control in a High-Speed Stage With Inlet Distortion: Part I—Radial Distortion," ASME J. Turbomach., **121**, pp. 510–516.
[25] Suder, K. L., Hathaway, M. D., Thorp, S. A., Strazisar, A. J., and Bright, M. M., 2001, "Compressor Stability Enhancement Using Discrete Tip Injection," ASME J. Turbomach., **123**, pp. 14–23.
[26] Adamczyk, J. J., Celestina, M. L., and Greitzer, E. M., 1993, "The Role of Tip Clearance in High-Speed Fan Stall," ASME J. Turbomach., **115**, pp. 28–38.
[27] Weigl, H. J., Paduano, J. D., Frechette, L. G., Epstein, A. H., Greitzer, E. M., Bright, M. M., and Strazisar, A. J., 1998, "Active Stabilization of Rotating Stall and Surge in a Transonic Single Stage Axial Compressor," ASME J. Turbomach., **120**(4), pp. 625–636.